

Formation of $\text{Al}_{15}\text{Mn}_3\text{Si}_2$ Phase During Solidification of a Novel Al-12%Si-4%Cu-1.2%Mn Heat-Resistant Alloy and Its Thermal Stability

Xiaojing Suo, Hengcheng Liao, Yiyun Hu, Uday S. Dixit, and Pavel Petrov

(Submitted October 14, 2016; in revised form December 2, 2017; published online February 21, 2018)

The formation of $\text{Al}_{15}\text{Mn}_3\text{Si}_2$ phase in Al-12Si-4Cu-1.2Mn (wt.%) alloy during solidification was investigated by adopting CALPHAD method and microstructural observation by optical microscopy, SEM–EDS, TEM–EDS/SAD and XRD analysis; SEM fixed-point observation method was applied to evaluate its thermal stability. As-cast microstructural observation consistently demonstrates the solidification sequence of the studied alloy predicted by phase diagram calculation. Based on the phase diagram calculation, SEM–EDS, TEM–EDS/SAD and XRD analysis, as well as evidences on Al–Si–Mn–Fe compounds from the literature, the primary and eutectic Mn-rich phases with different morphologies in the studied alloy are identified to be $\text{Al}_{15}\text{Mn}_3\text{Si}_2$ that has a body-centered cubic (BCC) structure with a lattice constant of $a = 1.352$ nm. SEM fixed-point observation and XRD analysis indicate that $\text{Al}_{15}\text{Mn}_3\text{Si}_2$ phase has more excellent thermal stability at high temperature than that of CuAl_2 phase and can serve as the major strengthening phase in heat-resistant aluminum alloy that has to face a high-temperature working environment. Results of tension test show that addition of Mn can improve the strength of Al–Si–Cu alloy, especially at elevated temperature.

Keywords heat-resistant aluminum alloy, microstructure, phase evolution, solidification, thermal stability

1. Introduction

Al–Si–Cu-based alloys have been extensively used to produce pistons, engine blocks and cylinder heads, due to low density, excellent cast ability, good mechanical properties as well as low cost (Ref 1–3). However, since the main strengthening phases in Al–Si–Cu-based alloys, such as CuAl_2 or Mg_2Si , usually are very prone to coarsening or even dissolving at above 443 K (170 °C), the conventional Al–Si–Cu system heat-resistant alloys cannot sustain or possess good strength at high temperature beyond 523 K (250 °C); thus, they cannot meet the increasingly more rigorous requirements of heat resistance for high power density engines (Ref 4–6). A great number of attempts have been made by several researchers to improve these promising alloys for high-temperature application (Ref 7–12). Zheng et al. (Ref 12) reported that the Cu content and Cu/Mg ratio had an considerable influence on the strength and ductility of Al–Si–Cu–Mg alloy because they affected the formation of primary

intermetallic phases during solidification and precipitates during heat treatment course. It was also reported that the mechanical properties of Al–Si–Cu–Mg alloys could be improved by increasing Mg and Cu contents (Ref 13, 14). Choi et al. (Ref 15) studied the effect of solution treatment of Al–Si–Cu–Mg alloy on mechanical and thermal characteristics and reported an improvement in tensile strength and thermal diffusivity. According to a report by Shaha et al. (Ref 4), addition of Cr, Zr, Ti and V could improve the elevated temperature strength of Al–Si–Cu–Mg alloy.

Mn is a common alloying element in aluminum alloy. Mn could enhance the high-temperature strength and creep resistance of aluminum alloy by forming high melting compounds, such as $\text{Cu}_2\text{Mn}_3\text{Al}_{20}$, $\text{Mn}_3\text{NiAl}_{16}$ or $\text{Al}_{15}(\text{Fe}, \text{Mn})_3\text{Si}_2$ (Ref 16). Qian et al. (Ref 17) reported an improvement in the elevated temperature tensile strength with the addition of Mn in ZL109. Similarly, it is reported that the Mn-rich dispersed precipitates formed during T6 heat treatment enhanced performance of the Mn-modified Al–Si–Cu–Mg alloy (Ref 18). Therefore, to meet the more rigorous requirements of heat resistance of aluminum alloys for high power density engine, Liao et al. (Ref 19) developed a novel heat-resistant casting alloys by adding high amount of Mn in near-eutectic Al–Si–Cu alloy, for an example, Al-12Si-4Cu-1.2Mn (wt.%). However, the formation of Mn-rich intermetallic phase in Al–Si–Cu–Mn alloy and its thermal stability have not been deeply studied.

The objective of this study is to characterize the Mn-rich intermetallic phase formed during solidification of Al-12Si-4Cu-1.2Mn (wt.%) alloy by CALPHAD method, combined with microstructural observation by optical microscopy, SEM and TEM as well as XRD analysis. In addition, SEM fixed-point observation method is applied to evaluate its thermal stability at high temperature. Mechanical properties at room temperature and elevated temperature are also discussed as well as tensile fractography.

Xiaojing Suo, Hengcheng Liao, and Yiyun Hu, School of Materials Science and Engineering, Southeast University, Jiangsu Key Laboratory for Advanced Metallic Materials, 2# Dongnandaxue Road, Nanjing 211189, China; Uday S. Dixit, Department of Mechanical Engineering, IIT Guwahati, Guwahati, Assam 781039, India; and Pavel Petrov, Department of Metal Forming and Metal Forming Machines, University of Mechanical Engineering, Moscow, Russian Federation 107023. Contact e-mails: suo_xj@163.com and hengchengliao@seu.edu.cn.

Table 1 Chemical composition of the studied alloy

Alloy	Element, wt.%					
	Si	Cu	Fe	Mn	Sr	Al
C1	11.98	3.92	0.169	1.24	0.0267	Balance
C2	11.80	3.90	0.157	...	0.0221	Balance

2. Experimental Procedure

The studied alloys were prepared in a graphite crucible of 3-kg capacity using a melting/vacuum holding furnace with Al-12.5 wt.%Si, Al-10 wt.%Sr and Al-10 wt.%Mn master alloys, commercial purity Cu (99.8 wt.%) ingot and Si (98 wt.%) particles. After processing, the melt was poured at 993 K (720 °C) into a plate-like iron mold (with a cavity of $170 \times 100 \times 20 \text{ mm}^3$, preheated at 523 K (250 °C) for 5 h). The final chemical composition of the prepared alloys was analyzed using MAXx LMF15 spark emission spectrometer, as listed in Table 1.

Metallographic samples were cut from the casting and were etched with a mixed acid reagent (20 mL HCl + 20 mL HNO₃ + 5 mL HF + 55 mL H₂O) for 15 s. Microstructural observation was carried out using Olympus BX60 M metallographic microscope, scanning electron microscope (SEM) equipped with EDS and transmission electron microscope (TEM) equipped with EDS and SAD. The x-ray diffraction (XRD, D8-Discover equipped with Cu-K_α radiation) was used to analyze phase constitutes with $2\theta = 10\text{--}55^\circ$ and a scanning step of $0.02^\circ/\text{step}$. Heat treatment of the sample used for SEM fixed-point observation was as follows: solutionizing at 798 K (525 °C) for 20 h, followed by the quenching in water at 298 K (25 °C).

Heat treatment of the samples used for tension test is as: solutionizing at 783 K (510 °C) for 5 h, then quenching in warm water at 298 K (25 °C), followed by artificially aging at 438 K (165 °C) for 6 h (i.e., T6 tempered). The tension test samples were pulled to fracture at a rate of 1 mm/min using CMT5105 electronic universal testing machine, and the test temperature is selected as 298 K (25 °C), 423 K (150 °C), 473 K (200 °C) and 523 K (250 °C). The fracture elongation was measured as the percent elongation (%EL) over the 35 mm gauge length, and the ultimate tensile strength (UTS) was obtained from the data acquisition system. The average %EL or UTS values obtained from the five test samples were considered as the value representing a specified condition.

3. Results and Discussion

3.1 Thermodynamic Phase Diagram Calculation

The phase diagram is helpful to understand the solidification path and phase evolution of an alloy system. Figure 1 shows the phase diagram of Al-12 wt.%Si-4 wt.%Cu-xMn (x from 0 to 1.5 wt.%) system calculated by Pandat™ software. The Mn content of the red line in Fig. 1 is 1.2 wt.%, which is the chemical composition of C1 alloy. In Fig. 1, the line labeled as

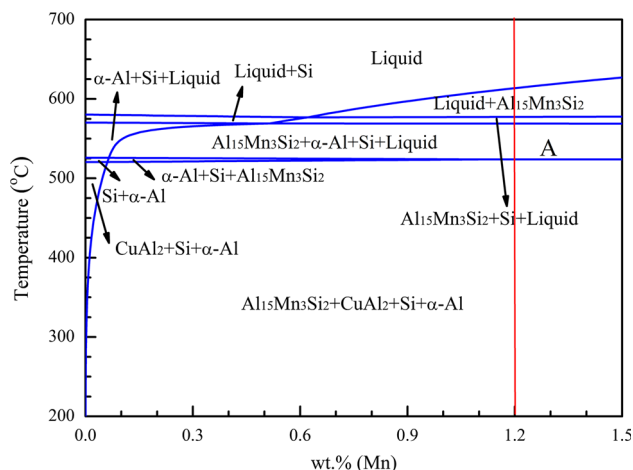


Fig. 1 The phase diagram of Al-12 wt.% Si-4 wt.% Cu-xMn (x from 0 to 1.5 wt.%) system calculated by Pandat™ software

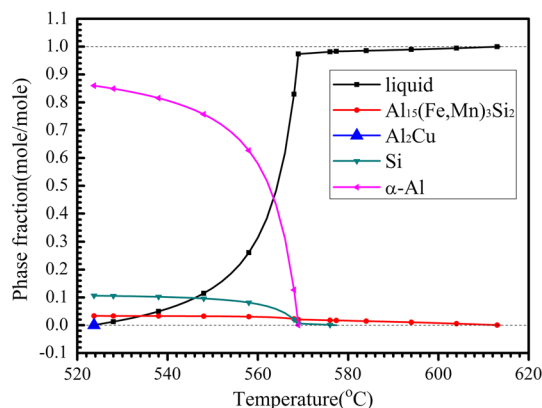


Fig. 2 Phase fraction of different phases calculated on Scheil model during solidification of the Al-12Si-4Cu-1.2 Mn (wt.%) alloy

“A” represents a quaternary isothermal eutectic reaction, namely liquid \rightarrow Al₁₅Mn₃Si₂ + α -Al + Si + CuAl₂. Figure 2 shows the phase fraction of different phases in C1 alloy during solidification, calculated by Pandat™ software on Scheil model. The phase transformations of C1 alloy during solidification are summarized in Table 2. For C1 alloy, when liquid temperature is dropped to 887 K (614 °C), the primary phase Al₁₅Mn₃Si₂ begins to crystallize from the liquid. This transformation continues to 850 K (577 °C). This primary Al₁₅Mn₃Si₂ phase grows as dendrites, depending on its crystallography characteristics. Then, binary eutectic of Al₁₅Mn₃Si₂ + Si forms from

Table 2 Phase transformation of C1 alloy during solidification

Reaction temperature, °C	Phase transformation
614-577	Liquid \rightarrow Al ₁₅ Mn ₃ Si ₂
577-569	Liquid \rightarrow Al ₁₅ Mn ₃ Si ₂ + Si
569-524	Liquid \rightarrow Al ₁₅ Mn ₃ Si ₂ + Si + α -Al
524	Liquid \rightarrow Al ₁₅ Mn ₃ Si ₂ + Si + α -Al + Al ₂ Cu

850 K (577 °C) to 842 K (569 °C), namely liquid \rightarrow Al₁₅Mn₃Si₂ + Si. From 842 K (569 °C) to 797 K (524 °C), ternary eutectic reaction occurs to form ternary eutectic of Al₁₅Mn₃Si₂ + α -Al + Si, namely liquid \rightarrow Al₁₅Mn₃Si₂ + α -Al + Si. At 797 K (524 °C), a quaternary eutectic reaction, namely liquid \rightarrow Al₁₅Mn₃Si₂ + α -Al + Si + CuAl₂, occurs at constant temperature to form quaternary eutectic of Al₁₅Mn₃Si₂ + α -Al + Si + CuAl₂ until all of the liquid is exhausted.

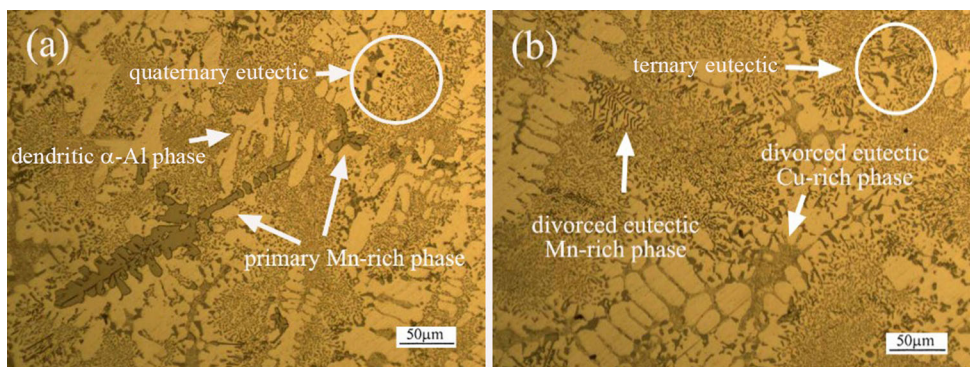


Fig. 3 Optical micrographs of as-cast microstructure of C1 alloy. (a) Primary Mn-rich phase and quaternary eutectic; (b) divorced eutectic Mn-rich phase, divorced eutectic Cu-rich phase and ternary eutectic

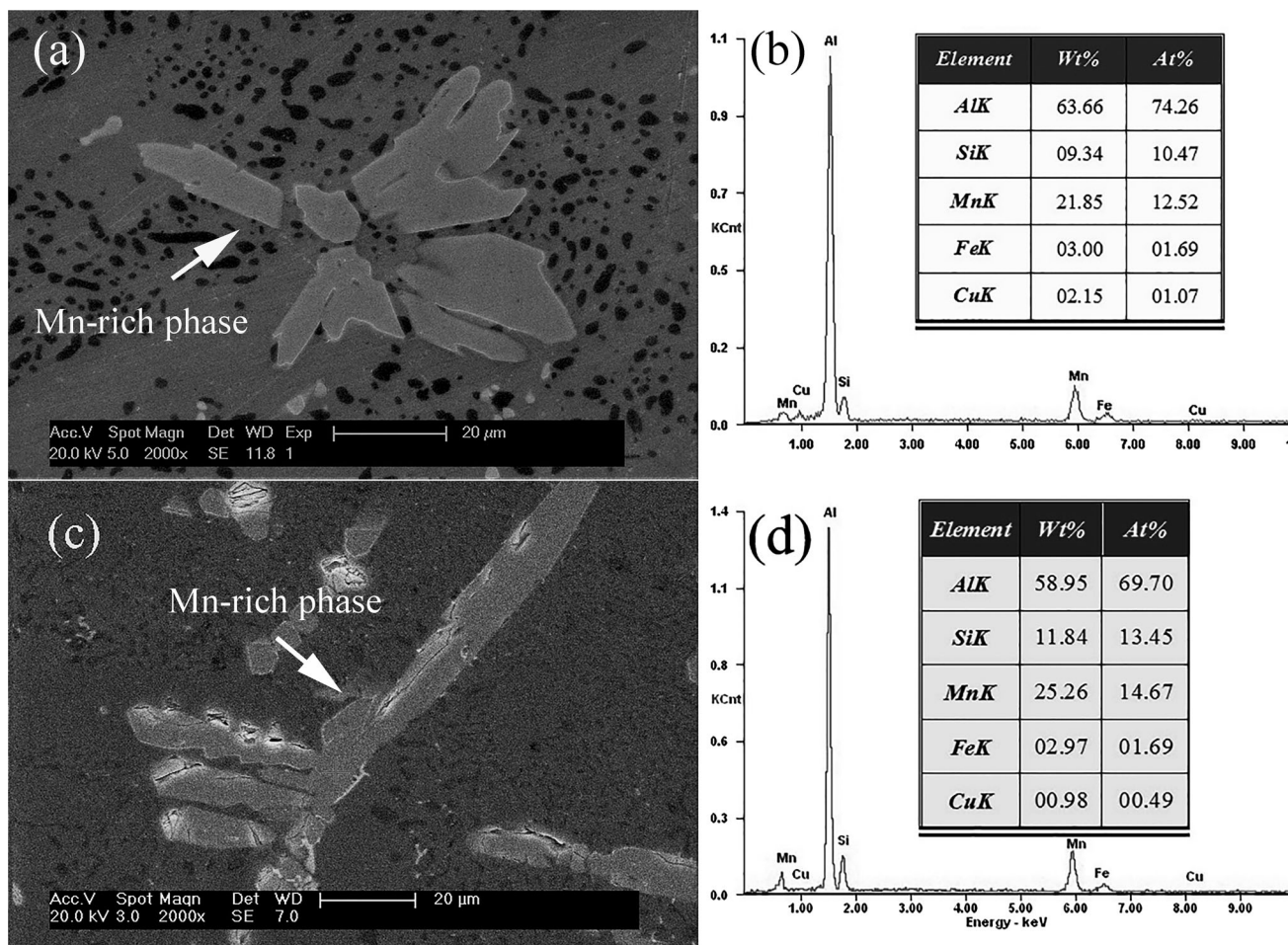


Fig. 4 SEM micrographs and EDS analysis of primary Mn-rich phase. (a, b) Dendrite arm; (c, d) dendrite trunk

3.2 As-Cast Microstructure

Figure 3 shows the optical micrographs of as-cast microstructure of C1 alloy. It is composed of primary Mn-rich phase dendrites, ternary eutectic of Mn-rich phase + α -Al + Si and quaternary eutectic of Mn-rich phase + Cu-rich phase + α -Al + Si. Based on the results of phase diagram calculation, binary eutectic of Mn-rich phase + Si should also

be included. However, it is not observed in the as-cast microstructure of C1 alloy, which may be due to two principal reasons. The first is that the crystallization range of binary eutectic is extremely narrow and hence its fraction is almost negligible. The other is that it is of great difficulty to distinguish the binary eutectic from the ternary eutectic. Therefore, it is assumed that the binary eutectic is also included. It is observed that there are some α -Al dendrites, which is due to non-

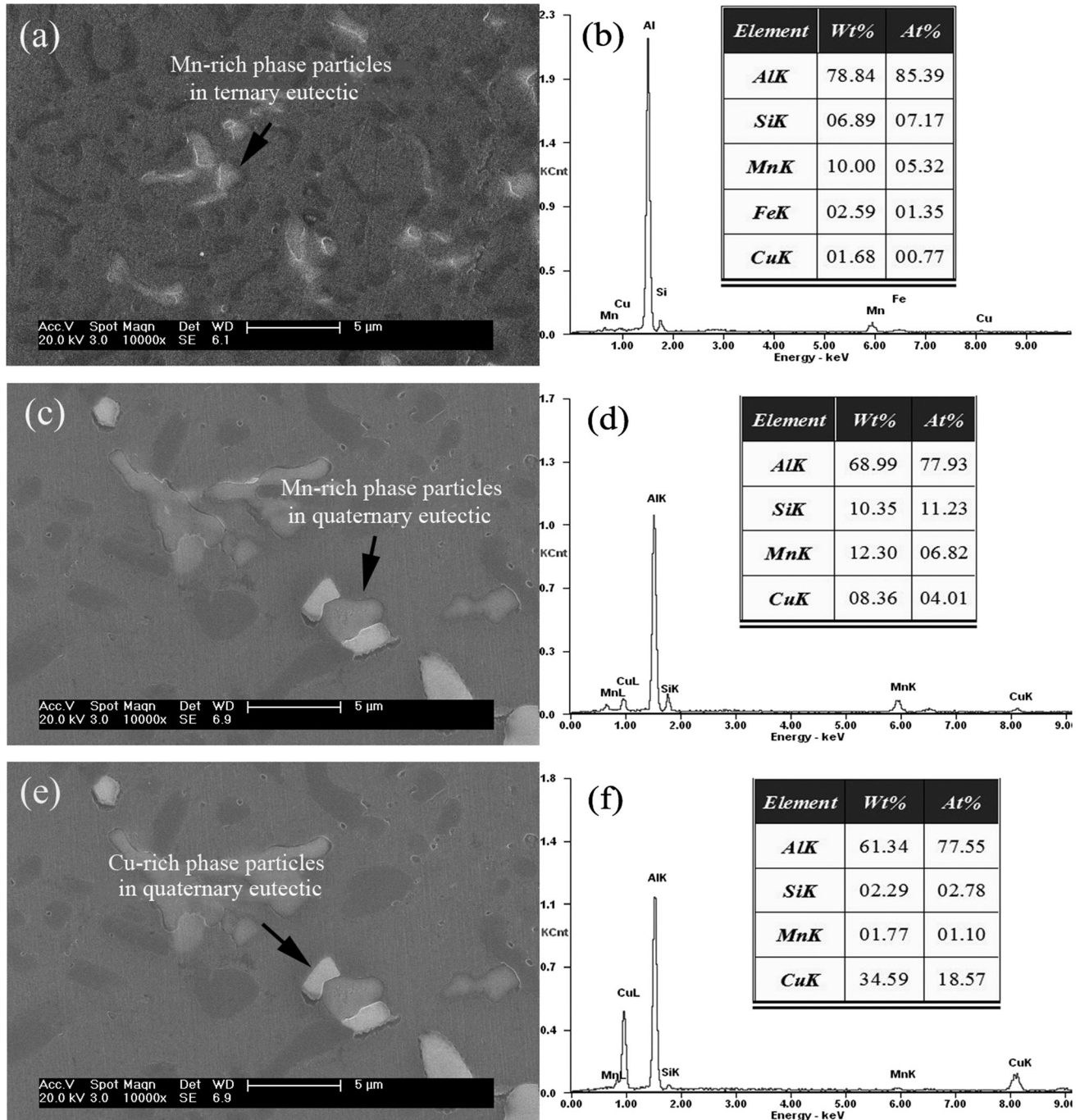


Fig. 5 SEM micrographs and EDS analysis of eutectic phases. (a, b) Mn-rich phase particles in ternary eutectic; (c, d) Mn-rich phase particles in quaternary eutectic; (e, f) Cu-rich particles in quaternary eutectic; (g, h) divorced eutectic Mn-rich phase with fishbone-like shape; (i, j) divorced Cu-rich phase with network-like shape

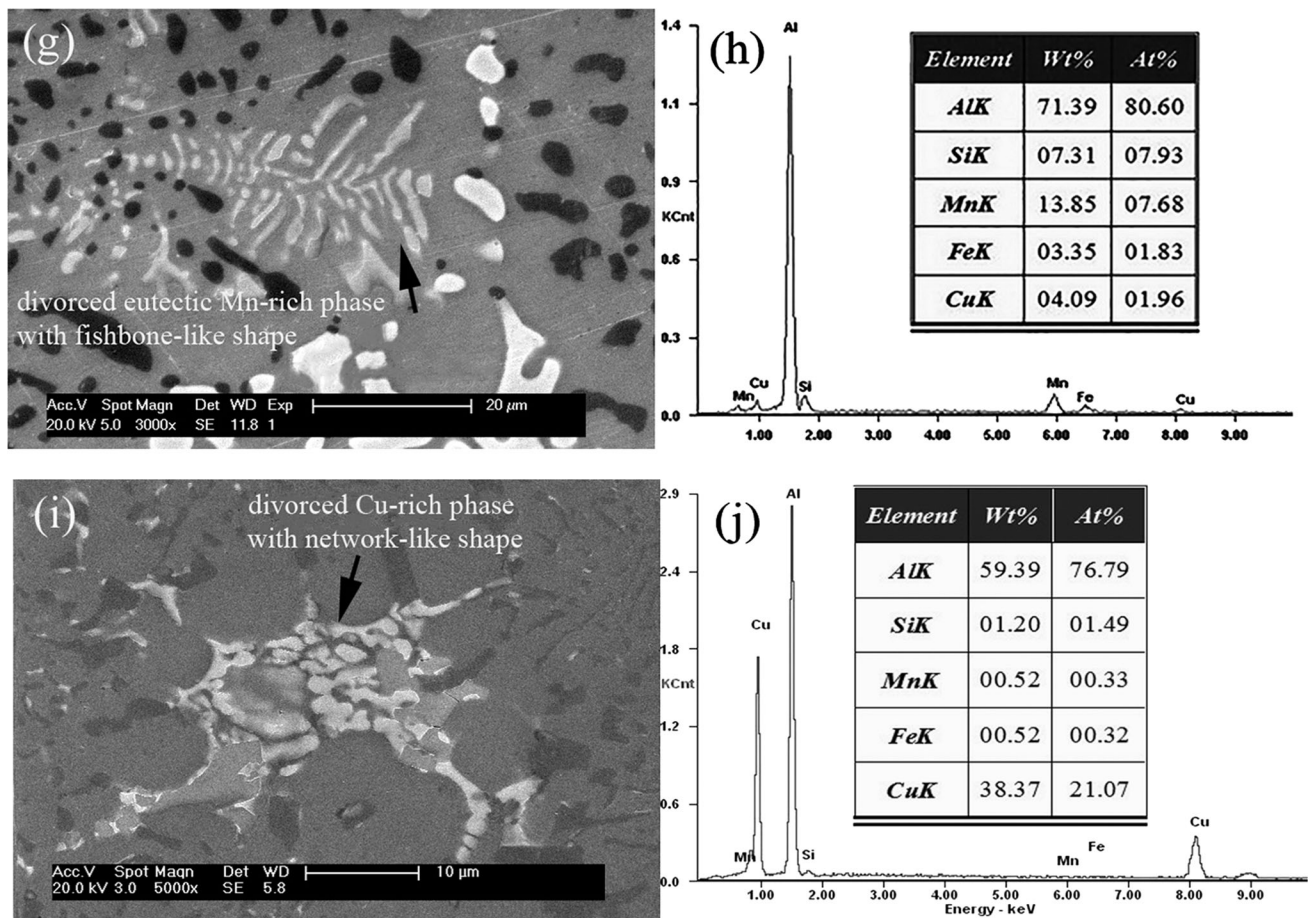


Fig. 5 continued

equilibrium solidification. Similarly, divorced eutectic Mn-rich phase with fishbone-like shape and divorced eutectic Cu-rich phase with network-like shape are also observed (as shown in Fig. 3b).

Figure 4 shows the EDS composition of dendrite arm and trunk of the primary Mn-rich phase, indicating that it is a ternary compound of Al, Si and Mn. Figure 5(a, b, c, and d) shows the composition of Mn-rich phase in ternary eutectic and quaternary eutectic, respectively. Figure 5(e and f) shows the constituents of Cu-rich phase in quaternary eutectic, while Fig. 5(g), (h), (i), and (j) shows the constituents of the divorced Mn-rich and Cu-rich eutectic phases, respectively. It is found that the primary Mn-rich phase dendrites, Mn-rich particles in both ternary and quaternary eutectics and divorced Mn-rich phase with fishbone-like shape have similar compositions, suggesting that they are the same ternary compounds of Al, Si and Mn. The divorced Cu-rich phase with network-like shape and Cu-rich particles in quaternary eutectic also have the same constituents of Al and Cu.

Figure 6(a) shows the XRD analysis of as-cast C1 alloy. It contains α -Al, Si, CuAl_2 (PDF card No: 65-2695) and only one Mn-rich phases, i.e., $\text{Al}_5\text{Si}_7\text{Mn}_{12}$ (PDF card No: 06-0669). It

indicates that primary Mn-rich phase dendrites, Mn-rich particles in binary, ternary and quaternary eutectics and divorced Mn-rich phase with fishbone-like shape are the same one of Al-Si-Mn ternary compound. Both the divorced Cu-rich phase with network-like shape and Cu-rich particles in quaternary eutectic are CuAl_2 phase. Though Mn-rich phase identified by diffraction peaks in XRD diagram is $\text{Al}_5\text{Si}_7\text{Mn}_{12}$, its composition has a big difference with the results of SEM-EDS analysis on primary Mn-rich phase dendrites. Moreover, according to the phase diagram calculation, the primary Mn-rich phase and eutectic Mn-rich phase are stable $\text{Al}_{15}\text{Mn}_3\text{Si}_2$. However, it is not included in the database of PDF cards in our library. Barbosa et al. (Ref 20) also analyzed a similar Al-Si-Cu alloy by XRD, and the position of the diffraction peaks of $\text{Al}_{17}(\text{Fe}_{3.2}\text{Mn}_{0.8})_3\text{Si}_2$ in their report is almost the same as that of $\text{Al}_5\text{Si}_7\text{Mn}_{12}$ in Fig. 6(a). Due to Fe content being much more than Mn in the study of Barbosa et al., the α - $\text{Al}_{17}(\text{Fe}_{3.2}\text{Mn}_{0.8})_3\text{Si}_2$ is more likely to be α - $\text{Al}_{12}\text{Fe}_3\text{Si}_2$ or α - $\text{Al}_{15}(\text{Fe},\text{Mn})_3\text{Si}_2$ as reported in Ref 21-24.

Figure 7 shows TEM photograph of the primary Mn-rich phase and its selected area electron diffraction (SAD) pattern and EDS diagram. According to the EDS composition result, it

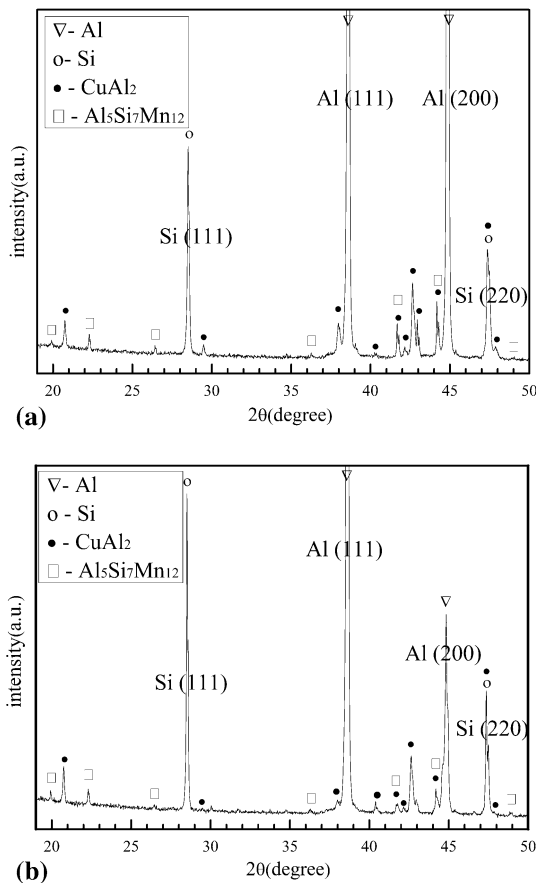


Fig. 6 XRD diagram of C1 alloy. (a) As cast; (b) as solutionized at 798 K (525 °C) for 20 h

could be crudely estimated as $\text{Al}_{20}\text{Mn}_2\text{Si}$, neglecting Fe and Cu. By SAD pattern, this Mn-rich phase is identified to have body-centered cubic (BCC) structure with a lattice constant of $a = 1.352$ nm. Shabestari (Ref 25) reported that the Al-Mn-Fe-Si intermetallic compound in the Al-Si-Cu-Mn system is $\text{Al}_{15}(\text{Fe},\text{Mn})_3\text{Si}_2$ and perceived that it has a cubic structure with a lattice parameter from $a = 1.265$ nm at 0 wt.% Fe to 1.25 nm at 31 wt.% Fe. In the present study, C1 alloy has very low Fe content (0.169 wt.%). Here, according to the thermodynamic phase diagram calculation of Al-12 wt.%Si-4 wt.%Cu-xwt%Mn system, SEM-EDS, TEM-EDS/SAD, XRD analysis and the evidences on Al-Si-Mn-Fe compound from the literature (Ref 20-25), the primary and eutectic Mn-rich phase is identified as $\text{Al}_{15}\text{Mn}_3\text{Si}_2$.

3.3 Thermal Stability of CuAl_2 and $\text{Al}_{15}\text{Mn}_3\text{Si}_2$ Phase

Fixed-point observation method by SEM is applied to evaluate the thermal stability of CuAl_2 and $\text{Al}_{15}\text{Mn}_3\text{Si}_2$ phase. In this method, microhardness indentation is used as a mark of location. Figure 8 shows the result of fixed-point observation of CuAl_2 phase in quaternary eutectic of C1 alloy. It can be seen that, after heating at 798 K (525 °C) for 20 h, the eutectic

CuAl_2 is partially re-dissolved, resulting in a significant reduction of the amount of CuAl_2 phase, whereas the survived CuAl_2 phase becomes granular and coarsened. It is consistent with the results of XRD analysis of C1 alloy before and after solution treatment. The diffraction peak intensity of CuAl_2 after solution treatment (Fig. 6b) is much less than that of as-cast state (Fig. 6a), but the peak does not disappear completely, which indicates that CuAl_2 dissolves partially during solution treatment. According to the present analysis, it is difficult for CuAl_2 phase to serve as the main heat-resistant phase of alloy at a higher temperature.

Figure 9 shows the result of the fixed-point observation on primary $\text{Al}_{15}\text{Mn}_3\text{Si}_2$ phase and eutectic $\text{Al}_{15}\text{Mn}_3\text{Si}_2$ phase in C1 alloy. It can be observed that there is no obvious change in size and shape of primary and eutectic $\text{Al}_{15}\text{Mn}_3\text{Si}_2$ phases. Similarly, the diffraction peak intensity of $\text{Al}_{15}\text{Mn}_3\text{Si}_2$ phase does not change obviously after the solution treatment process (Fig. 6). This confirms that $\text{Al}_{15}\text{Mn}_3\text{Si}_2$ phase has more excellent thermal stability at high temperature compared to CuAl_2 phase and hence can serve as the major strengthening phase in heat-resistant aluminum alloy that has to face a high working temperature.

3.4 Mechanical Properties at Room Temperature and Elevated Temperature

The tensile properties at room temperature and elevated temperature of two alloys (C1 with 1.2%Mn and C2 without Mn) are shown in Table 3 and Fig. 10. As shown in Fig. 10, both the C1 alloy and the C2 alloy show a decrease in UTS and an increase in EL% with the test temperature. It can also be seen that the UTS values of C1 alloy at different test temperature are evidently higher than that of the C2 alloy. This confirms that the C2 alloy has been strengthened by Mn addition. When the test temperature is higher than 473 K (200 °C), there is a sharp decrease in the UTS of C2 alloy about 48 MPa, while the change of the UTS of C1 alloy is much smaller, only about 10 MPa, indicating the new introduced $\text{Al}_{15}\text{Mn}_3\text{Si}_2$ phase can remarkably improve the elevated temperature strength of the alloy.

3.5 Fractography

To better understand the failure mechanism of the alloys at room temperature and elevated temperature, the fracture surfaces of the tensile samples of C1 and C2 alloys were examined using SEM, as shown in Fig. 11 and 12. It can be seen that the fracture surfaces of both C1 and C2 alloys illustrate mixed-rupture characteristics of cleavage and dimples, which indicates the brittle and ductile fracture coexists in the alloys. The area of the cleavage planes increases obviously with the Mn addition. For C1 alloy (with Mn), the cleavage planes at 250 °C have high amount of Mn (as shown in Fig. 12a, b, c, and d), which shows Mn-rich phases result in a stress concentration in the surrounding matrix and provide easy path for fracture. From another point of view, just the Mn-rich phases undertake the loading at high temperature. For C2 alloy (without Mn), the fracture surfaces are dominated by ductile

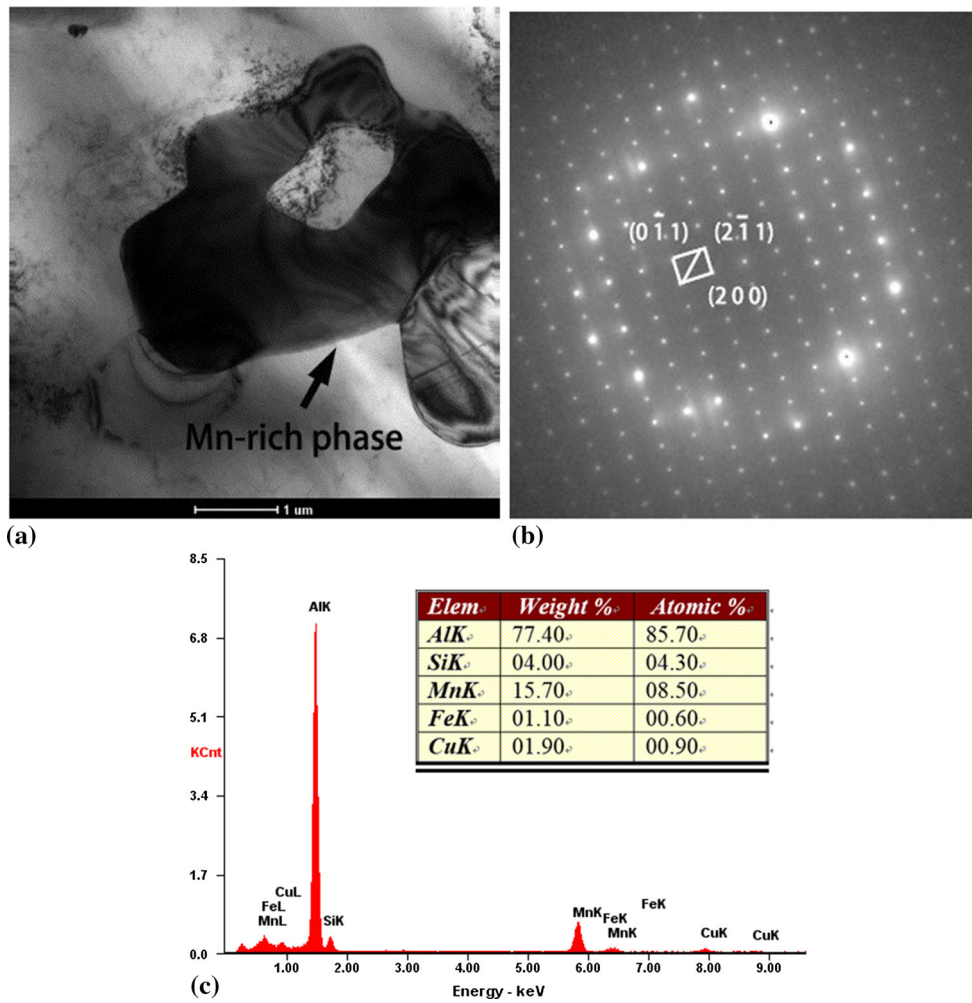


Fig. 7 TEM photograph of the primary Mn-rich phase in as-cast microstructure of C1 alloy (a), its SAD pattern at the zone axis $B = [011]$ (b) and EDS analysis (c)

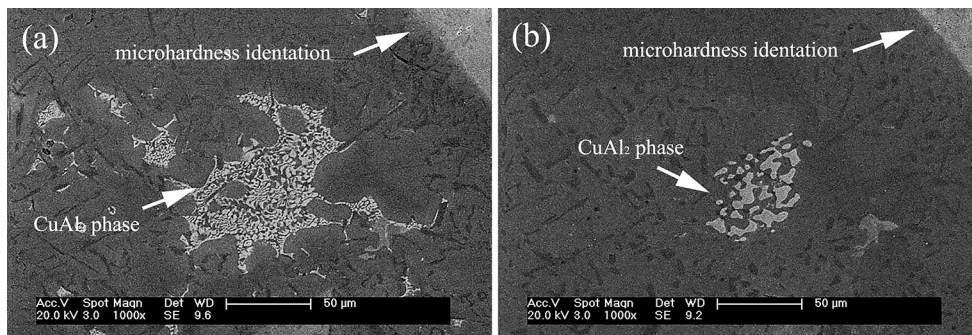


Fig. 8 SEM micrographs of the fixed-point observation of CuAl₂ phase in quaternary eutectic of C1 alloy. (a) As cast; (b) as solutionized at 798 K (525 °C) for 20 h

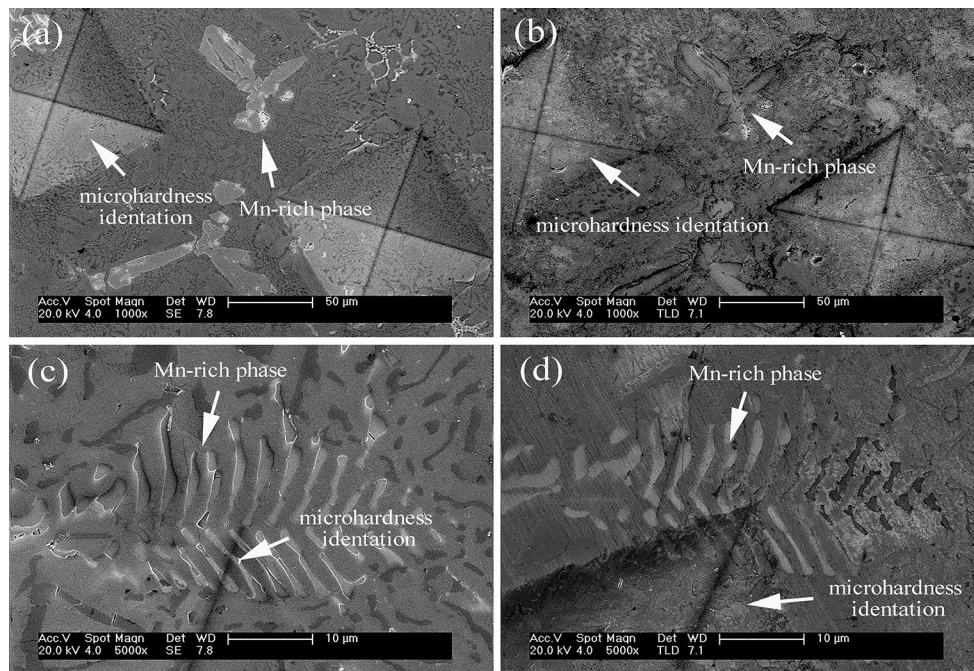


Fig. 9 SEM micrographs of the fixed-point observation of $\text{Al}_{15}\text{Mn}_3\text{Si}_2$ phase in C1 alloy. (a, b) Primary $\text{Al}_{15}\text{Mn}_3\text{Si}_2$ phase as cast and as solutionized (at 798 K (525 °C) for 20 h), respectively; (c, d) divorced eutectic $\text{Al}_{15}\text{Mn}_3\text{Si}_2$ phase as cast and as solutionized (at 798 K (525 °C) for 20 h), respectively

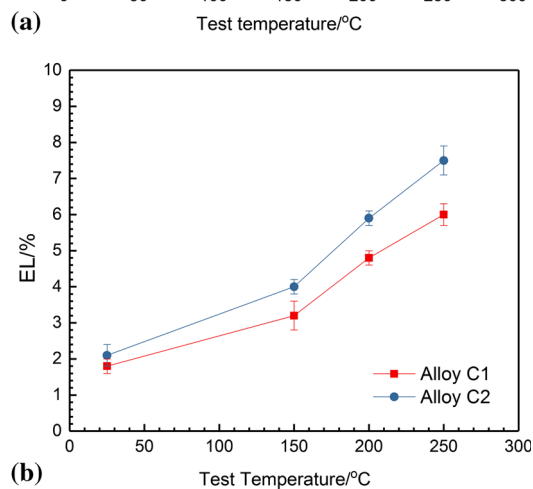
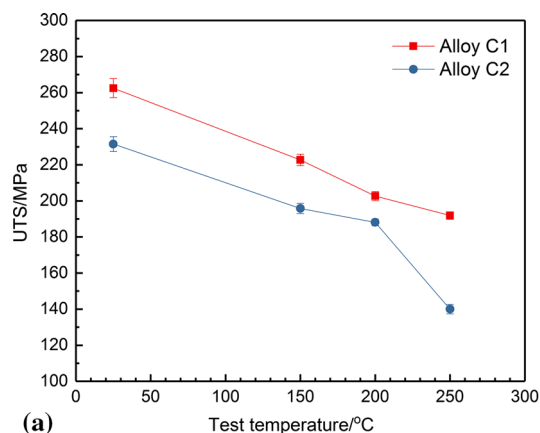


Fig. 10 Temperature dependence of (a) ultimate tensile strength and (b) fracture elongation of C1 and C2 alloys

Table 3 Tensile properties at room and elevated temperature

Alloy	Test temperature, °C	UTS, MPa (T6)	EL, %
C1	25	262.5 ± 5.3	1.8 ± 0.2
	150	222.7 ± 3.2	3.2 ± 0.4
	200	202.7 ± 2.5	4.8 ± 0.2
	250	191.9 ± 2.1	6.0 ± 0.3
	250	191.9 ± 2.1	6.0 ± 0.3
C2	25	231.5 ± 4.1	2.1 ± 0.3
	150	195.8 ± 2.8	4.0 ± 0.2
	200	188.1 ± 1.8	5.9 ± 0.2
	250	140.0 ± 2.6	7.5 ± 0.4
	250	140.0 ± 2.6	7.5 ± 0.4

transcrystalline with dimples, and the cleavage planes at both room temperature and 250 °C have the constituents of Al, Cu and Fe (as shown in Fig. 12e, f, g, and h), possibly being CuAl_2 phase.

4. Conclusions

Based on the present study, the following conclusions are drawn:

- (1) As-cast microstructure of Al-12Si-4Cu-1.2Mn (wt.%) alloy consistently demonstrates the solidification sequence predicted by phase diagram calculation.
- (2) Based on the phase diagram calculated by Pandat™, SEM-EDS, TEM-EDS/SAD, XRD analysis and combined evidences on Al-Si-Mn-Fe compound from the literature, the primary and eutectic Mn-rich phases with different morphologies in Al-12Si-4Cu-

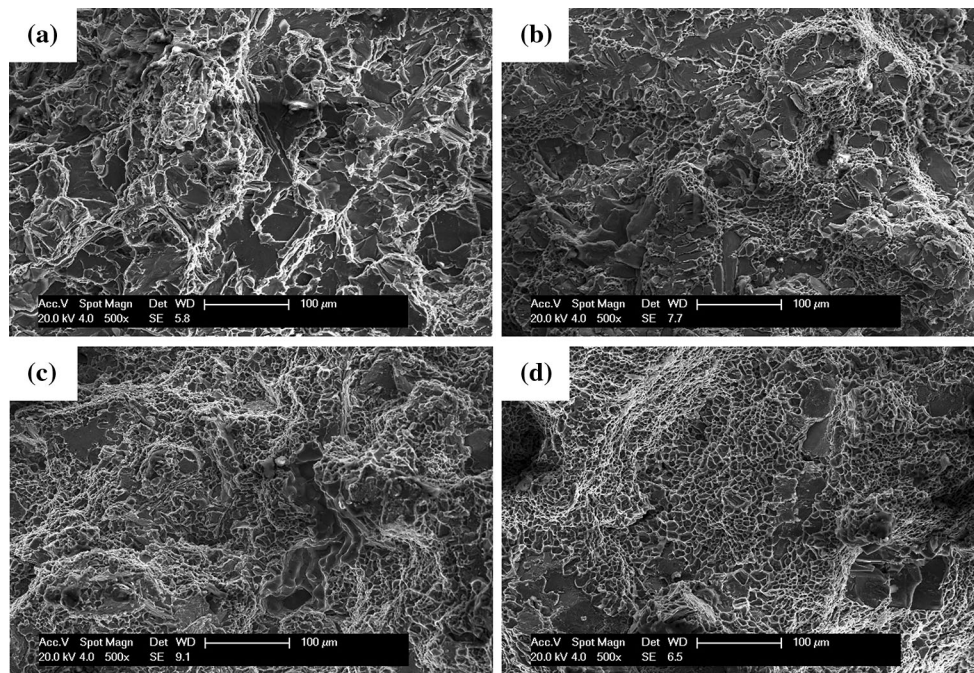


Fig. 11 SEM images of the fracture surfaces of the tensile samples. (a) C1 alloy at room temperature; (b) C1 alloy at 250 °C; (c) C2 alloy at room temperature; (d) C2 alloy at 250 °C

1.2Mn (wt.%) alloy are identified to be $\text{Al}_{15}\text{Mn}_3\text{Si}_2$ that has a body-centered cubic (BCC) structure with a lattice constant of $a = 1.352$ nm.

- (3) Results of SEM fixed-point observation and XRD analysis show that $\text{Al}_{15}\text{Mn}_3\text{Si}_2$ phase has more excellent thermal stability at a high temperature compared to CuAl_2

phase and hence can serve as the major strengthening phase in heat-resistant aluminum alloy that has to face a high working temperature.

- (4) Results of tension test indicate that addition of Mn can considerably improve the tensile strength of Al-Si-Cu alloy, especially at elevated temperature.

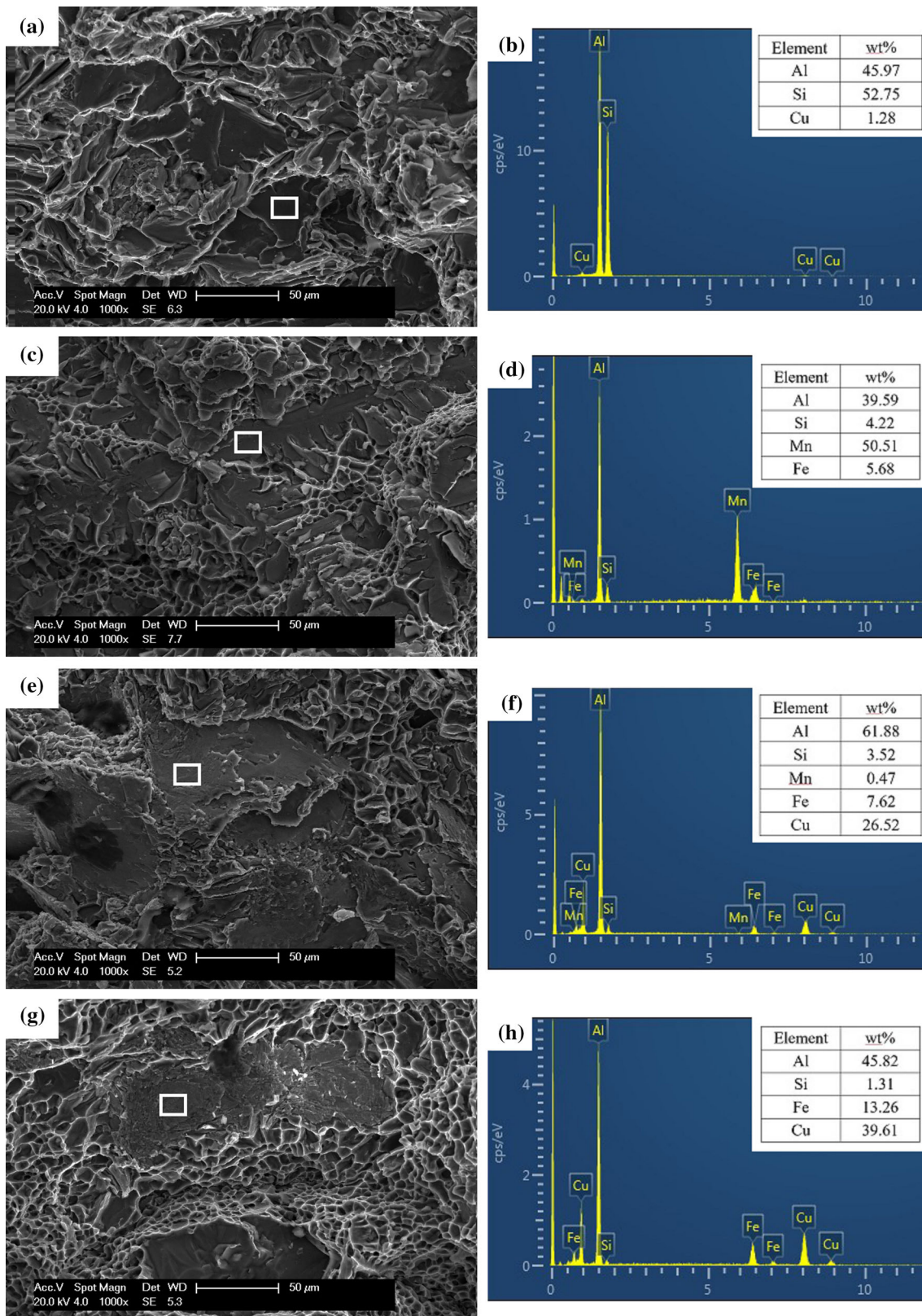


Fig. 12 SEM images and EDS analysis of the fracture surfaces of the tensile samples. (a, b) C1 alloy at room temperature; (c, d) C1 alloy at 250 °C; (e, f) C2 alloy at room temperature; (g, h) C2 alloy at 250 °C

Acknowledgments

This work is supported by Jiangsu Key Laboratory of Advanced Metallic Materials (BM2007204) and the Fundamental Research Funds for the Central Universities (2242016K40011).

References

1. M.M. Haque and A. Sharif, Study on Wear Properties of Aluminium-Silicon Piston Alloy, *J. Mater. Process. Technol.*, 2001, **118**(1–3), p 69–73
2. Y. Wu, J. Zhang, H. Liao, G. Li, and Y. Wu, Development of High Performance Near Eutectic Al-Si-Mg Alloy Profile by Micro Alloying with Ti, *J. Alloys Compd.*, 2016, **660**, p 141–147 (in English)
3. H. Liao, Y. Sun, and G. Sun, Correlation Between Mechanical Properties and Amount of Dendritic α -Al Phase in As-Cast Near-Eutectic Al-11.6% Si Alloys Modified with Strontium, *Mater. Sci. Eng. A*, 2002, **335**(1–2), p 62–66 (in English)
4. S.K. Shaha, F. Czerwinski, W. Kasprzak, J. Friedman, and D.L. Chen, Ageing Characteristics and High-Temperature Tensile Properties of Al-Si-Cu-Mg Alloys with Micro-Additions of Cr, Ti, V and Zr, *Mater. Sci. Eng. A*, 2016, **652**, p 353–364 (in English)
5. A.R. Farkoosh, M. Javidani, M. Hoseini, D. Larouche, and M. Pekguleryuz, Phase Formation In As-Solidified and Heat-Treated Al-Si-Cu-Mg-Ni Alloys: Thermodynamic Assessment and Experimental Investigation for Alloy Design, *J. Alloys Compd.*, 2013, **551**, p 596–606 (in English)
6. P. Sepehrband, R. Mahmudi, and F. Khomamizadeh, Effect of Zr Addition on the Aging Behavior of A319 Aluminum Cast Alloy, *Scr. Mater.*, 2005, **52**(4), p 253–257 (in English)
7. A.R. Farkoosh, X.G. Chen, and M. Pekguleryuz, Dispersoid Strengthening of a High Temperature Al-Si-Cu-Mg Alloy via Mo Addition, *Mater. Sci. Eng. A*, 2015, **620**, p 181–189 (in English)
8. A.R. Farkoosh and M. Pekguleryuz, The Effects of Manganese on the T-Phase and Creep Resistance in Al-Si-Cu-Mg-Ni Alloys, *Mater. Sci. Eng. A*, 2013, **582**, p 248–256 (in English)
9. A.M.A. Mohamed, A.M. Samuel, F.H. Samuel, and H.W. Doty, Influence of Additives on the Microstructure and Tensile Properties of Near-Eutectic Al-10.8%Si Cast Alloy, *Mater. Des.*, 2009, **30**(10), p 3943–3957 (in English)
10. A.R. Farkoosh and M. Pekguleryuz, Enhanced Mechanical Properties of an Al-Si-Cu-Mg Alloy at 300 °C: Effects of Mg and the Q-Precipitate Phase, *Mater. Sci. Eng. A*, 2015, **621**, p 277–286 (in English)
11. P. Huter, P. Renhart, S. Oberfrank, M. Schwab, F. Grün, and B. Stauder, High- and Low-Cycle Fatigue Influence of Silicon, Copper, Strontium and Iron on Hypo-Eutectic Al-Si-Cu and Al-Si-Mg Cast Alloys Used in Cylinder Heads, *Int. J. Fatigue*, 2016, **82**, p 588–601 (in English)
12. Y. Zheng, W. Xiao, S. Ge, W. Zhao, S. Hanada, and C. Ma, Effects of Cu Content and Cu/Mg Ratio on the Microstructure and Mechanical Properties of Al-Si-Cu-Mg Alloys, *J. Alloys Compd.*, 2015, **649**, p 291–296 (in English)
13. A.M.A. Mohamed, F.H. Samuel, and S. Al kahtani, Influence of Mg and Solution Heat Treatment on the Occurrence of Incipient Melting in Al-Si-Cu-Mg Cast Alloys, *Mater. Sci. Eng. A*, 2012, **543**, p 22–34 (in English)
14. M.S. Salleh, M.Z. Omar, and J. Syarif, The Effects of Mg Addition on the Microstructure and Mechanical Properties of Thixoformed Al-5%Si-Cu Alloys, *J. Alloys Compd.*, 2015, **621**, p 121–130 (in English)
15. S.W. Choi, Y.M. Kim, K.M. Lee, H.S. Cho, S.K. Hong, Y.C. Kim, C.S. Kang, and S. Kumai, The Effects of Cooling Rate and Heat Treatment on Mechanical and Thermal Characteristics of Al-Si-Cu-Mg Foundry Alloys, *J. Alloys Compd.*, 2014, **617**, p 654–659 (in English)
16. H. Yang, S. Ji, and Z. Fan, Effect of Heat Treatment and Fe Content on the Microstructure and Mechanical Properties of Die-Cast Al-Si-Cu Alloys, *Mater. Des.*, 2015, **85**, p 823–832 (in English)
17. Z. Qian, X. Liu, D. Zhao, and G. Zhang, Effects of Trace Mn Addition on the Elevated Temperature Tensile Strength and Microstructure of a Low-Iron Al-Si Piston Alloy, *Mater. Lett.*, 2008, **62**, p 2146–2149 (in English)
18. S.K. Shaha, F. Czerwinski, W. Kasprzak, J. Friedman, and D.L. Chen, Effect of Mn and Heat Treatment on Improvements in Static Strength and Low-Cycle Fatigue Life of an Al-Si-Cu-Mg Alloy, *Mater. Sci. Eng. A*, 2016, **657**, p 441–452 (in English)
19. H. Liao, Y. Tang, X. Suo, G. Li, Y. Hu, U.S. Dixit, and P. Petrov, Dispersoid Particles Precipitated During the Solutionizing Course of Al-12 wt.%Si-4 wt.%Cu-1.2 wt.%Mn Alloy and Their Influence on High Temperature Strength, *Mater. Sci. Eng. A*, 2017, **699**, p 201–209 (in English)
20. J. Barbosa, H. Puga, J. Oliveira, S. Ribeiro, and M. Prokic, Physical Modification of Intermetallic Phases in Al-Si-Cu Alloys, *Mater. Chem. Phys.*, 2014, **148**, p 1163–1170 (in English)
21. K. Liu, X. Cao, and X.-G. Chen, Tensile Properties of Al-Cu 206 Cast Alloys with Various Iron Contents, *Metall. Mater. Trans. A*, 2014, **45**, p 2498–2507 (in English)
22. W. Zhang, B. Lin, J. Fan, D. Zhang, and Y. Li, Microstructures and Mechanical Properties of Heat-Treated Al-5.0Cu-0.5Fe Squeeze Cast Alloys with Different Mn/Fe Ratio, *Mater. Sci. Eng. A*, 2013, **588**, p 366–375 (in English)
23. E.R. Wang, X.D. Hui, and G.L. Chen, Eutectic Al-Si-Cu-Fe-Mn Alloys with Enhanced Mechanical Properties at Room and Elevated Temperature, *Mater. Des.*, 2011, **32**, p 4333–4340 (in English)
24. G. Gustafsson, T. Thorvaldsson, and G.L. Dunlop, The Influence of Fe and Cr on the Microstructure of Cast Al-Si-Mg Alloys, *Metall. Mater. Trans. A*, 1986, **17**, p 45–52 (in English)
25. S.G. Shabestari, The Effect of Iron and Manganese on the Formation of Intermetallic Compounds in Aluminum-Silicon Alloys, *Mater. Sci. Eng. A*, 2004, **383**, p 289–298 (in English)